CellPress

Structure
Short Article

Structures of Yeast 80S Ribosome-tRNA Complexes in the Rotated and Nonrotated Conformations

Egor Svidritskiy,[1,4] Axel F. Brilot,[2,4] Cha San Koh,[1] Nikolaus Grigorieff,[2,3,5,*] and Andrei A. Korostelev[1,5,*]
[1]RNA Therapeutics Institute, Department of Biochemistry and Molecular Pharmacology, University of Massachusetts Medical School, 368 Plantation Street, Worcester, MA 01605, USA
[2]Department of Biochemistry, Rosenstiel Basic Medical Sciences Research Center, Brandeis University, Waltham, MA 02454, USA
[3]Janelia Farm Research Campus, Howard Hughes Medical Institute, 19700 Helix Drive, Ashburn, VA 20147, USA
[4]Co-first author
[5]Co-senior author
*Correspondence: niko@grigorieff.org (N.G.), andrei.korostelev@umassmed.edu (A.A.K.)
http://dx.doi.org/10.1016/j.str.2014.06.003

SUMMARY

The structural understanding of eukaryotic translation lags behind that of translation on bacterial ribosomes. Here, we present two subnanometer resolution structures of *S. cerevisiae* 80S ribosome complexes formed with either one or two tRNAs and bound in response to an mRNA fragment containing the Kozak consensus sequence. The ribosomes adopt two globally different conformations that are related to each other by the rotation of the small subunit. Comparison with bacterial ribosome complexes reveals that the global structures and modes of intersubunit rotation of the yeast ribosome differ significantly from those in the bacterial counterpart, most notably in the regions involving the tRNA, small ribosomal subunit, and conserved helix 69 of the large ribosomal subunit. The structures provide insight into ribosome dynamics implicated in tRNA translocation and help elucidate the role of the Kozak fragment in positioning an open reading frame during translation initiation in eukaryotes.

INTRODUCTION

The translation of genetic information to a protein sequence is performed by ribosomes in all organisms. Although the functional sites of the ribosome, such as the decoding center and the peptidyl transferase center, are universally conserved, there are substantial differences between bacterial and eukaryotic translation, as reflected in distinct mechanisms of initiation, termination, and ribosome recycling (Aitken and Lorsch, 2012; Dever and Green, 2012).

Translation initiation plays an important role in gene expression regulation in homeostasis, cell stress, development, and disease (Sonenberg and Hinnebusch, 2009). In bacteria, translation initiation depends on three initiation factors and results in the formation of a 70S ribosome complex with initiator tRNA formylmethionine ($tRNA^{fMet}$) bound in the P site in response to the AUG codon (Myasnikov et al., 2009). The Shine-Dalgarno sequence upstream of the open reading frame (Dalgarno and Shine, 1973) forms base-pairing interactions with the complimentary anti-Shine-Dalgarno region of the ribosomal 16S RNA. The formation of this specific contact results in positioning of the downstream AUG start codon in the P site of the small 30S subunit, thus determining the open reading frame of the mRNA for translation (Kaminishi et al., 2007; Korostelev et al., 2007; Yusupova et al., 2006). By contrast, initiation in eukaryotes depends on at least a dozen initiation factors (Aitken and Lorsch, 2012). An mRNA region termed the Kozak consensus sequence flanking the AUG start codon is required for efficient translation initiation (Kozak, 1986). The context around the start codon is therefore considered to be critical for selection of the correct AUG start codon among several possible AUG trinucleotides at the 5′ end of an mRNA. Although the Kozak sequence is variable among groups of eukaryotes, in vertebrates, the sequence is strongly biased toward containing purines at positions −3 and +4 relative to A+1 of the AUG start codon (Cavener and Ray, 1991). Mutation of a purine to pyrimidine at position −3 has been shown to have the most detrimental effect on the efficiency of translation compared with mutations at other positions (Kozak, 1986). In nonvertebrate eukaryotes, the most stringent requirement is that a nucleotide at position −3 is a purine, whereas the conservation and functional importance of the identity of the nucleotide at position +4 is less pronounced (Cavener and Ray, 1991). Despite suggestions that there is some analogy of the Kozak consensus and Shine-Dalgarno sequences based on their locations, the Kozak sequence likely does not act by forming base-pairing interactions with 18S ribosomal RNA. First, the variability of the Kozak sequence among eukaryotes does not correlate with the high conservation of the eukaryotic 18S ribosomal RNA. Second, the 3′ end of 18S rRNA of most species does not contain sequences that would be strongly complementary to the Kozak consensus (Verrier and Jean-Jean, 2000). Third, introducing complementarity between the untranslated 5′ region and the 3′ end of 18S rRNA leads to the inhibition of translation rather than enhancement (Verrier and Jean-Jean, 2000). As such, the molecular mechanism of the Kozak sequence function remains unknown.

Upon initiation, elongation of the polypeptide chain takes place. The cycle of elongation is accompanied by consecutive movement (translocation) of tRNAs and the respective mRNA codons from the A (aminoacyl) to the P (peptidyl) to the E (exit)

site. In studies of bacterial ribosomes, significant progress has been made in the structural and functional characterization of translocation intermediates, reflecting the key steps of translocation. Upon peptidyl transfer from the peptidyl tRNA to aminoacyl tRNA, translocation occurs in two consecutive steps. These are (1) the movement of the acceptor arms of the peptidyl and deacyl tRNAs from the A and P sites into the P and E sites on the large subunit (resulting in tRNAs adopting hybrid A/P and P/E conformations), followed by (2) movement of the anticodon stem loops into the P and E sites on the small subunit, catalyzed by elongation factor G (in bacteria) or eEF-2 (in eukaryotes). Crystallographic and electron cryomicroscopy (cryo-EM) structures as well as solution experiments helped establish that, during translation, the ribosome undergoes large-scale conformational changes. The most pronounced is the intersubunit rotation (Frank and Agrawal, 2000) coupled with formation of hybrid states by tRNAs (Ermolenko et al., 2007; Moazed and Noller, 1989; Spiegel et al., 2007). The ribosome adopts a nonrotated state when tRNAs are located in the classical A, P, and E sites. The small subunit rotates relative to the large subunit by ~9° when tRNAs adopt hybrid A/P and P/E states. Importantly, the ribosome and tRNAs fluctuate spontaneously between the nonrotated (classical) and rotated (hybrid) states, independent of elongation factors, emphasizing that the formation of translocation intermediates is an inherent property of the ribosome (Cornish et al., 2008). In addition to intersubunit rotation, large-scale intrasubunit rearrangements take place, including (1) rotation of the head of the small subunit (Guo and Noller, 2012; Ratje et al., 2010), which allows widening of the mRNA-tRNA corridor between the P and E sites (Schuwirth et al., 2005), and (2) movement of the L1 stalk, which interacts with the tRNA elbow as tRNA progresses from the P/E to the E state (Cornish et al., 2009; Fei et al., 2008).

The structural understanding of eukaryotic translation lags behind that of bacterial translation. Some studies suggest that the dynamic behavior of eukaryotic ribosomes and tRNAs as well as their structural details may differ from those of their bacterial counterparts. Specifically, cryo-EM reconstructions of vacant eukaryotic ribosomes revealed that eukaryotic ribosomes predominantly adopt a rotated conformation, unlike vacant bacterial ribosomes, which predominantly sample the nonrotated state (Cornish et al., 2008; Spahn et al., 2004). Furthermore, the predominant conformations of eukaryotic ribosomes bound with elongation factor eEF-2 and endogenous tRNA found near the E site (Anger et al., 2013) differ from those of bacterial ribosomes bound with EF-G and tRNA sampling the hybrid P/E states (Brilot et al., 2013; Frank and Agrawal, 2000; Pulk and Cate, 2013; Tourigny et al., 2013; Zhou et al., 2013) or the classical P state (Gao et al., 2009). To understand the mechanism of translocation on eukaryotic ribosomes, a detailed structural reconstruction of 80S translocation intermediates is required. Although a number of tRNA- and elongation factor eEF2-bound eukaryotic complexes have been visualized by cryo-EM, the structural details of 80S ribosome dynamics and interactions with tRNA and mRNA remain poorly characterized for several reasons. These include insufficient resolution, compositional heterogeneity of complexes containing endogenous mixtures of mRNA and tRNA, and, until recently, the absence of a high-resolution crystal structure of the eukaryotic ribosome that could be used for structural comparisons. A 3 Å crystal structure of the yeast 80S ribosome in the absence of tRNA and mRNA has been determined recently (Ben-Shem et al., 2011), allowing for detailed model building and interpretation of cryo-EM structures. Concurrently, pretranslocation mammalian ribosomes assembled with defined mRNA and tRNA were visualized by cryo-EM at 9–10.6 Å resolution (Budkevich et al., 2011). The latter structures revealed that, in the presence of the A-site tRNA, the pretranslocation ribosome adopts the rotated and nonrotated states, coupled with tRNAs adopting the hybrid and classical states, respectively. The positions of the P- and E-site tRNAs in the nonrotated ribosome have been reported to differ significantly from those in the bacterial ribosomes. It remained unclear, however, whether the A-site tRNA plays a role in inducing such differences. To reconstruct the structural pathway of translocation on the 80S ribosome, additional complexes are required to be visualized, including the posttranslocation ribosome containing tRNA in the P and E sites as well as other tRNA-bound intermediates that may provide insights into ribosome dynamics.

In this work, we present ~6 Å resolution cryo-EM structures for two compositionally homogeneous tRNA-bound *S. cerevisiae* 80S complexes formed with a defined mRNA construct containing the *S. cerevisiae* Kozak consensus fragment. Improvements in cryo-EM data classification (Lyumkis et al., 2013) and the use of the 80S ribosome crystal structure (Ben-Shem et al., 2011) refined against our cryo-EM maps allow us to present detailed structural models of the 80S•2tRNA and 80S•tRNA complexes. Comparison of the 80S structures with those of the bacterial counterparts provides insights into the kingdom-specific structural aspects of translocation. In addition, our structures provide insights into the role of the Kozak fragment in positioning the open reading frame on the ribosome. Specifically, the structures suggest that the Kozak sequence works, at least in part, as a molecular ruler, allowing placement of the AUG codon in the P site, because of interactions of the Kozak sequence elements with the conserved structures of the small ribosomal subunit.

RESULTS AND DISCUSSION

We have assembled *S. cerevisiae* 80S ribosome complexes in the presence of initiator $tRNA^{fMet}$ and an mRNA fragment that includes an authentic *S. cerevisiae* Kozak fragment preceding the AUG start codon, as described in Experimental Procedures. To ensure compositional homogeneity, vacant ribosomes free of endogenous tRNA (Ben-Shem et al., 2011) were purified prior to complex assembly. Cryo-EM classification of 80S particles (Figure S1 available online) revealed two main 80S classes at ~6 Å resolution, accounting for nearly 60% of particles (Figure 1). The quality of both maps allowed the interpretation of the protein and RNA secondary structure. In the core of the ribosome, which is most highly ordered, it is possible to interpret the phosphate backbone and individual bulged or stacked nucleotides. We used real-space refinement to accurately fit the 3 Å crystal structure of the *S. cerevisiae* ribosome into the cryo-EM maps essentially as described previously (Koh et al., 2014) (Figures 1C and 1D). Class I comprises nonrotated 80S ribosomes, bound with two tRNA molecules, in the P and E sites (80S•2tRNA; Figure 1A). Class II represents rotated 80S

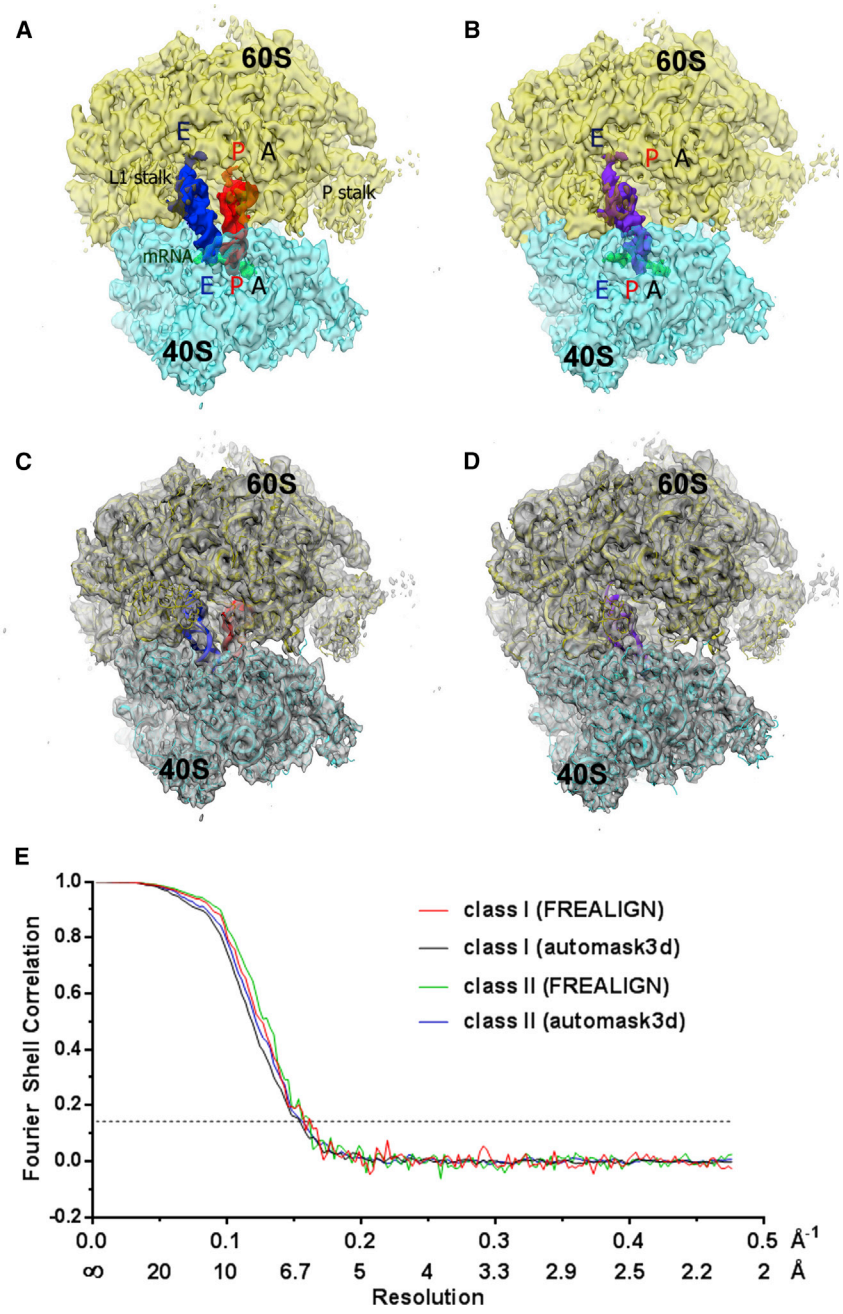

Figure 1. Cryo-EM Reconstructions of the 80S Ribosome

(A and B) Cryo-EM maps of the ribosome bound with (A) two tRNAs and (B) single tRNA. The large 60S subunit is shown in yellow/orange, the small 40S subunit in cyan, the E-site tRNA molecule in blue, the P-site tRNA molecule in red, and hybrid P/E tRNA in purple.

(C and D) Molecular structures of the ribosome refined into the maps shown in (A) and (B). Colors are as shown in (A) and (B).

(E) Fourier shell correlation (FSC) curves for classes representing the 80S•2tRNA and 80S•tRNA complexes (I and II, respectively). The FSC was calculated using automask3d, and FREALIGN for each class was generated as described under Experimental Procedures. For convenience, the x axis is labeled with spatial frequency $Å^{-1}$ and with Å. The resolution stated in the text corresponds to an FSC cutoff value of 0.143, shown as a dotted line, for the FREALIGN-derived FSC.

ribosomes bound with a single tRNA in the hybrid P/E state (80S•tRNA; Figure 1B).

Structure of the Nonrotated 80S Ribosome Bound with Two tRNAs

The complex with two tRNAs bound in the P and E sites of the nonrotated ribosome represents a posttranslocation-like state of eukaryotic ribosomes. Comparison of our 80S•2tRNA ribosome structure with the bacterial 70S ribosome bound with two tRNAs (Jenner et al., 2010) reveals two global differences. First, the small subunit is significantly tilted relative to the large 60S subunit (Figure 2A). The tilt of the subunit as a whole places the head of the small 40S subunit up to 7 Å farther away from the core of the large subunit than in the bacterial ribosome. The tilt is coupled with displacement of the intersubunit bridge B1b (Yusupov et al., 2001) formed by the proteins S18 (S13 in bacteria) at the head of the 40S subunit and L11 (L5 in bacteria) at the central protuberance of the large subunit (Figure 2B). Here, the position of the central protuberance, whose core is formed by 5S ribosomal RNA, relative to the core of the large subunit is different from that in the bacterial ribosome. This protrusion of the central protuberance as a whole results from the eukaryote-specific expansion segments 31ES9 (stemming from helix 31), 38ES12 (stemming from helix 38, also known as the A site finger) and elongated helix 30 (Petrov et al., 2014). These extensions displace 5S ribosomal RNA and the associated L11 toward the small subunit (Figures 2B and 2C). In summary, the addition of the eukaryote-specific ribosomal RNA expansion segments next to 5S rRNA results in displacement of the central protuberance toward the small subunit, resulting in the tilting of the latter.

The second significant difference between eukaryotic and bacterial ribosomes is in the positions of the tRNAs in the classical P and E sites. In the yeast ribosome, the P-site tRNA is located closer to the E site, whereas the E-site tRNA is closer to the P site (Figure 2D). This brings the elbows of tRNAs in the 80S complex ~15 Å closer together than in the bacterial ribosome (Korostelev et al., 2006; Selmer et al., 2006). Our analysis of the kingdom-specific structural differences suggests that the positioning of the P-site tRNA is influenced by the placement of the central protuberance with which the tRNA interacts via L11

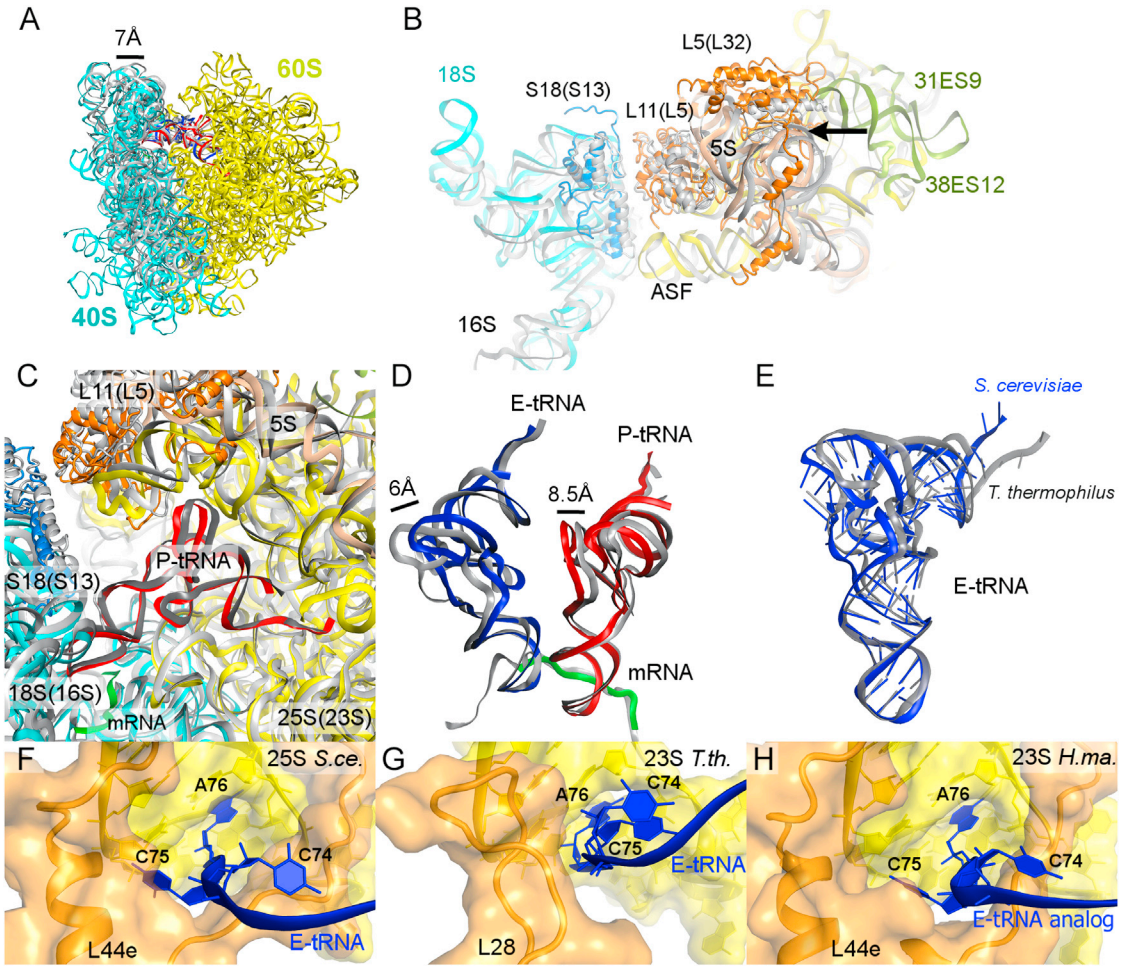

Figure 2. Structural Differences between tRNA-Bound Nonrotated 80S Yeast Ribosomes and Ribosomes from Other Kingdoms of Life

(A) The tilt of the small subunit relative to the large subunit induced by eukaryote-specific expansion segments of 25S ribosomal RNA, resulting in the shift of the head of the small subunit away from the core of the large subunit by up to 7 Å. Ribosomal proteins are not shown for clarity. A comparison of the position of 18S ribosomal RNA in the nonrotated 80S (this work) with that of 16S ribosomal RNA in *T. thermophilus* 70S ribosome (Jenner et al., 2010) bound with two tRNAs (PDB ID 3I9B) was obtained by structural alignment of 25S rRNA (yellow) and 23S rRNA (not shown).

(B) Displacement of bridge B1b, formed between the central protuberance of the large subunit and the head of the small subunit, in the 80S ribosome relative to that in the 70S ribosome (gray). The superposition was achieved by structural alignment of 25S rRNA of the 80S•2tRNA ribosome (this work) and 23S rRNA of the *T. thermophilus* 70S•2tRNA ribosome structure (Jenner et al., 2010). ASF, A site finger.

(C) Differences between the positions of P-site tRNAs in the yeast (red) and *T. thermophilus* (gray) ribosome structures, induced by different architectures of the central protuberance. The superposition was obtained as in (B) by aligning large-subunit rRNAs of corresponding structures (this work and Jenner et al., 2010).

(D) Conformational and positional differences between tRNAs bound to yeast (red and blue, this work) and bacterial *T. thermophilus* 70S ribosomes (gray, Jenner et al., 2010). Positions of E- and P-site tRNAs were compared by structural alignment of small-subunit rRNAs.

(E) Conformational difference between E-site tRNAs bound to yeast (blue, this work) and bacterial (gray; Jenner et al., 2010) ribosomes obtained by structural alignment of tRNA anticodon stem loops.

(F–H) Conformations of the 3′-CCA terminus of E-site tRNA bound to yeast (F, this work) and *T. thermophilus* (*T. th.*) (G, Jenner et al., 2010) ribosomes and an acceptor arm analog bound to the archaeal *H. marismortui* (*H. ma.*) 50S subunit (H, (Schmeing et al., 2003). The large subunit is shown in yellow (rRNA) and orange (proteins), the small subunit in cyan (18S) and marine (proteins), E-site tRNA in blue, P-site tRNA in red, mRNA in green, and eukaryote-specific elements of 25S rRNA in yellow/green. Elements of the 70S ribosome are shown in gray when compared with those of the 80S ribosome. *S. ce.*, *S. cerevisiae*.

(L5 in bacteria) (Figure 2C). In the E site, the elbow of the tRNA interacts with the L1 stalk (Figure S2). The difference in bacterial and eukaryotic E-site tRNA positions is likely caused by differences in the L1 stalk structures (Petrov et al., 2014). The L1 stalk of the yeast ribosome (Figures S2A and S2B) lacks helix 78, which, in bacterial ribosomes, approaches small subunit protein S11 (Figures S2C and S2D). Because the contact between the L1 stalk and the small subunit is absent in the nonrotated yeast ribosome, the L1 stalk and E-site tRNA elbow adopt different positions than in the bacterial ribosome.

We also investigated whether the distinct global conformations of the yeast and bacterial complexes are specific to the yeast ribosome or to the posttranslocation-like state of the 80S ribosome. To this end, we compared our structure with ~10 Å resolution, pretranslocation-like rabbit 80S ribosomes in which all the three tRNA sites are occupied by tRNAs (Budkevich

et al., 2011). We found that the positions of tRNAs in the P and E sites of these complexes are nearly identical, indicating that the occupancy of the A site does not influence the placement of the P- and E-site tRNAs. The similar positions of tRNAs in the yeast and mammalian ribosomes suggest that the tRNA positioning is conserved among eukaryotes.

The relative positions of ribosomal functional centers in the A, P, and E sites are nearly identical in bacterial and eukaryotic ribosomes. Our observation of different tRNA positions in the bacterial and eukaryotic ribosomes prompted us to also look for conformational differences within the tRNAs that could account for different positioning of the tRNAs relative to the similarly positioned functional centers. tRNAs are known to be highly flexible, and their conformational dynamics are thought to be critical for tRNA translocation through the ribosome, during which the acceptor arm and the CCA end sample different conformations relative to the anticodon stem loop (Caulfield et al., 2011). Superposition of tRNAs from our 80S structures with those of the bacterial 70S counterpart (Jenner et al., 2010) revealed that the classical P-site tRNA adopts nearly identical conformations. By contrast, the E-site tRNA adopts significantly different conformations in the 70S and 80S complexes. Specifically, the CCA end in the 80S complex is bent by ~20° relative to that in the bacterial complex (Figure 2E). The E-site tRNA interacts with the E site of the large subunit (Figure 2F), which, in eukaryotes, is compositionally and conformationally different from that in bacteria. In bacterial tRNA-bound ribosomes, the CCA 3′ end of the tRNA interacts with helix 82 of 23S rRNA and protein L28 (Korostelev et al., 2006; Selmer et al., 2006). The two cytosines of the CCA trinucleotide form a system of stacked nucleotides with the acceptor arm (Figure 2G). In our structure of the nonrotated 80S ribosome, the CCA end interacts with the conserved h82 (in the vicinity of C2765 and G2793) and with protein L44e, which is structurally distinct from bacterial L28. In contrast to the bacterial E-site tRNA structure, the penultimate nucleotide C75 of the tRNA appears unstacked from C74 and, instead, interacts with L44e in the vicinity of Tyr-43 (Figure 2F). In this conformation, the 3′ terminus of the tRNA and its interactions closely resemble those of a hairpin loop mimicking the tRNA acceptor arm in the 3.1 Å crystal structure (Figure 2H) of the archaeal 50S subunit (Schmeing et al., 2003), consistent with the phylogenetic conservation of L44e between eukaryotes and archaea. In summary, the phylogenetic differences in the composition of the E sites between bacteria and eukaryotes contribute to the diverged conformations of the tRNA bound in the E site.

Structure of the Rotated 80S Ribosome Bound with the P/E tRNA

Upon classification of cryo-EM images, the second most populated class contained a single deacylated tRNA. Structural studies of bacterial ribosomes bound with a deacylated tRNA have revealed a variety of inter- and intrasubunit rearrangements, providing important insights into the dynamics of the 70S ribosome (Agirrezabala et al., 2012). This prompted us to characterize the 80S•tRNA complex in detail. In the 80S•tRNA structure, the ribosome adopts a single rotated conformation in which the small subunit is rotated relative to that in the 80S•2tRNAs complex by ~8.5° (Figure 1B).

As in the analyses described above, we also compared the rotated 80S•tRNA ribosome and the crystal structure of its bacterial counterpart (Dunkle et al., 2011). We found significant differences in the positions of the small subunit, tRNA and helix 69 of the large subunit, which forms an intersubunit bridge next to the decoding center of the small subunit. These differences arise from the tilted position of the small subunit relative to the large subunit, resulting from the interaction between the protruding central protuberance and the 40S head (Figure 3A). The tilt of the small subunit in the rotated ribosome is more pronounced than that in the nonrotated structure (~6° versus ~3°). The tilt results in shifted positions of tRNA binding sites on the 40S subunit relative to the core of the 60S subunit in comparison with the sites in bacterial ribosomes. Specifically, the anticodon stem loop of P/E-site tRNA and helix 69 (h69) of the rotated 80S ribosome are shifted together with the small subunit by almost 6 Å toward to the E site in comparison with those in the bacterial ribosomes (Figure 3B). The rearrangement of h69 relative to the large subunit is, therefore, coupled with the movement of the small subunit with which h69 forms intersubunit bridge B2a (Yusupov et al., 2001).

We next asked whether the 80S ribosome with a single deacylated P/E tRNA is different from the rotated rabbit 80S ribosome in which two tRNAs are bound in the P/E and A/P states, respectively. Superposition of the large subunit ribosomal RNAs revealed that the global conformations of the yeast and mammalian ribosomes are similar, as well as the position of the P/E-site tRNA. This indicates that the occupancy of the A/P hybrid state does not affect the overall global conformation of the ribosome. The position of h69 in the mammalian ribosome structure (Budkevich et al., 2011) appears to be different from that in the yeast ribosome, perhaps because of the occupancy of the A site of the 40S subunit, which is located near h69. Therefore, it remains to be clarified whether h69 moves passively as the ribosome rearranges between the rotated and nonrotated states or is involved in A-site tRNA repositioning in the course of translocation.

Intersubunit Rotation of the 80S Ribosome

To gain insights into the mechanism of rotation of the small subunit between the nonrotated and rotated conformations, we compared our 80S•2tRNA and 80S•tRNA structures. Superposition of the large ribosomal subunit rRNA reveals an ~8.5° rotation of the small subunit, reminiscent of the range of rotation for bacterial ribosomes (Agirrezabala et al., 2008; Julián et al., 2008). The axis of rotation (Figure 3C) crosses the penultimate helix (h44) similarly to that in the bacterial system (Korostelev and Noller, 2007). Notably, the position of the rotation axis in the eukaryotic ribosome is distinct from that of the bacterial ribosome. In particular, the tilt of the upper part of the small subunit caused by the protruded central protuberance results in the tilt of the rotation axis by ~23° (Figure 3C), indicating that the detailed mode of rotation and rearrangement of intersubunit contacts is likely different in bacterial and eukaryotic ribosomes. Visualization of additional intermediates of the intersubunit rotation is required to further address the mechanism of intersubunit rearrangements.

In summary, the comparison of the rotated and nonrotated eukaryotic ribosome complexes with bacterial counterparts suggests that, although the subunits of ribosomes from both

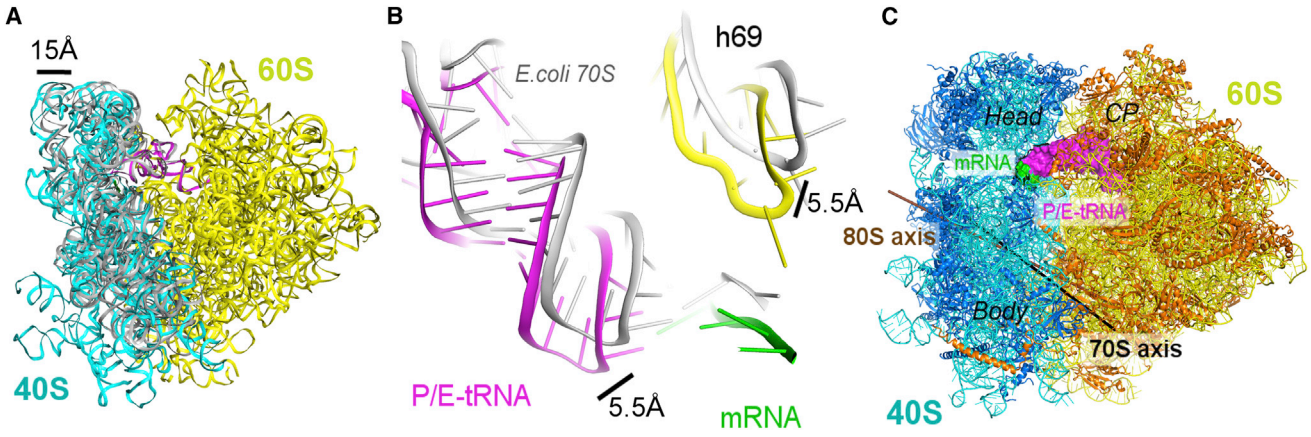

Figure 3. Differences in the Conformations of Rotated Yeast and Bacterial Ribosomes Bound with P/E-site tRNA

(A) The tilt of the small 40S subunit relative to the large 60S subunit, resulting in the shift of the head of the small subunit away from the core of the 60S subunit by up to 15 Å. Proteins are not shown for clarity. A comparison of the positions of 18S ribosomal RNA in the rotated 80S ribosome (this work) with *E. coli* 16S ribosomal RNA (Dunkle et al., 2011) was obtained by structural alignment of 25S rRNA (yellow) and 23S rRNA (not shown).

(B) Differences in position of the tRNA, mRNA, and helix 69 between the rotated yeast (this work) and *E. coli* (Dunkle et al., 2011) ribosomes. The superposition was obtained by structural alignment of large-subunit rRNA of the 80S and 70S complexes, respectively (not shown).

(C) Intersubunit rotation axes for yeast (brown) and *E. coli* (black) ribosomes. The rotation axis for each ribosome was calculated in Chimera (Pettersen et al., 2004) using the small subunit rRNA from nonrotated (bound with two tRNAs) and rotated (bound with single tRNA) ribosome structures. The superposition of yeast and bacterial (Dunkle et al., 2011) ribosome structures was obtained by structural alignment of large-subunit rRNAs. Head and body domains of the small subunit and the central protuberance (CP) of the large subunit are labeled. 60S is shown in yellow and orange, 40S in cyan and marine, 70S in gray, the 80S rotation axis in brown, and the 70S rotation axis in black.

kingdoms undergo a large-scale rotation, the detailed mode of the rotation is different. Our structures reveal kingdom-specific differences, including the previously unreported distinct dynamics of helix 69, coupled with rearrangements of the small subunit. It is possible that, in the globally similar pathways of bacterial and eukaryotic tRNA and mRNA translocation, the intermediates of ribosome rearrangements may be distinct between the two kingdoms. In turn, the similarity between the E-site architectures of eukaryotic and archaeal ribosomes suggests that the archaeal ribosomes and tRNAs sample the conformational states that are similar to eukaryotic but distinct from bacterial ribosomes. These kingdom-specific differences should be taken into account when parallels are drawn between the well studied bacterial and understudied archaeal and eukaryotic translation mechanisms.

The Kozak Sequence as a Molecular Ruler

The sequence context of the AUG start codon has been shown to be of key importance for the efficiency of translation initiation in eukaryotes and, therefore, for the selection of the open reading frame (Kozak, 1986). Although the sequence requirements (Kozak consensus) differ among eukaryotic species, the presence of a purine nucleotide at position −3 is the most stringent requirement in all eukaryotes (Cavener and Ray, 1991). Adenosine is thought to occupy this position in more than 70% of mRNAs and guanosine in more than 25% (Cavener and Ray, 1991). The structural role of this stringent requirement is not clear because it could not be addressed by previous structural studies of the 80S complexes because of low resolution and/or compositional heterogeneity of endogenous mRNA found in the ribosome. In our work, we used a fragment of mRNA that contains an authentic *S. cerevisiae* Kozak sequence, A***A***AA (Hamilton et al., 1987), immediately upstream of the AUG codon. The presence of the initiator tRNA base-paired with the AUG codon at the 40S P site in our maps indicates that the position of the mRNA fragment within the ribosome reflects that of a tRNA-bound initiation state of the 80S ribosome.

The density of mRNA in the A, P, and E sites is well resolved, allowing us to build and refine an mRNA model at the three tRNA-mRNA binding sites of the 40S subunit. The structures of mRNA are similar in the 80S•tRNA and 80S•2tRNA complexes. The three nucleotides immediately preceding the AUG codon are located in the E site (Figure 4A). The density in the E site is characteristic of stacked nucleotides and contains sufficient detail to identify phosphate groups. The positions and conformations of the nucleotides in the E site (Figure 4B) are similar to those found in the 3.1 Å resolution crystal structure of the bacterial 70S ribosome (Protein Data Bank ID 3I8G) (Jenner et al., 2010) in which the mRNA in the E site was well resolved (Figure 4C). The similarity between our mRNA model and the mRNA in the crystal structure of the 70S ribosome, as well as the stereochemically plausible packing of nucleotides within the density, suggest the following interactions. The adenosine of interest (A-3) is positioned to form stacking interactions with the universally conserved G904 (G693 in *E. coli*) located at the tip of hairpin loop 23 of the small ribosomal RNA. At the other side, A-3 stacks on A-2, as suggested by the similar contact in the high-resolution structure of the bacterial ribosome (Figure 4C). The bases of A-3 and A-2 are positioned next to the glycine-rich tip of a β hairpin of protein S5 (amino acids 152–154, Figure 4A). Our structural model is consistent with results of biochemical experiments showing that the nucleotide in position −3 crosslinks with G904 (Demeshkina et al., 2000) and S5 (Pisarev et al., 2006) in mammalian ribosomes.

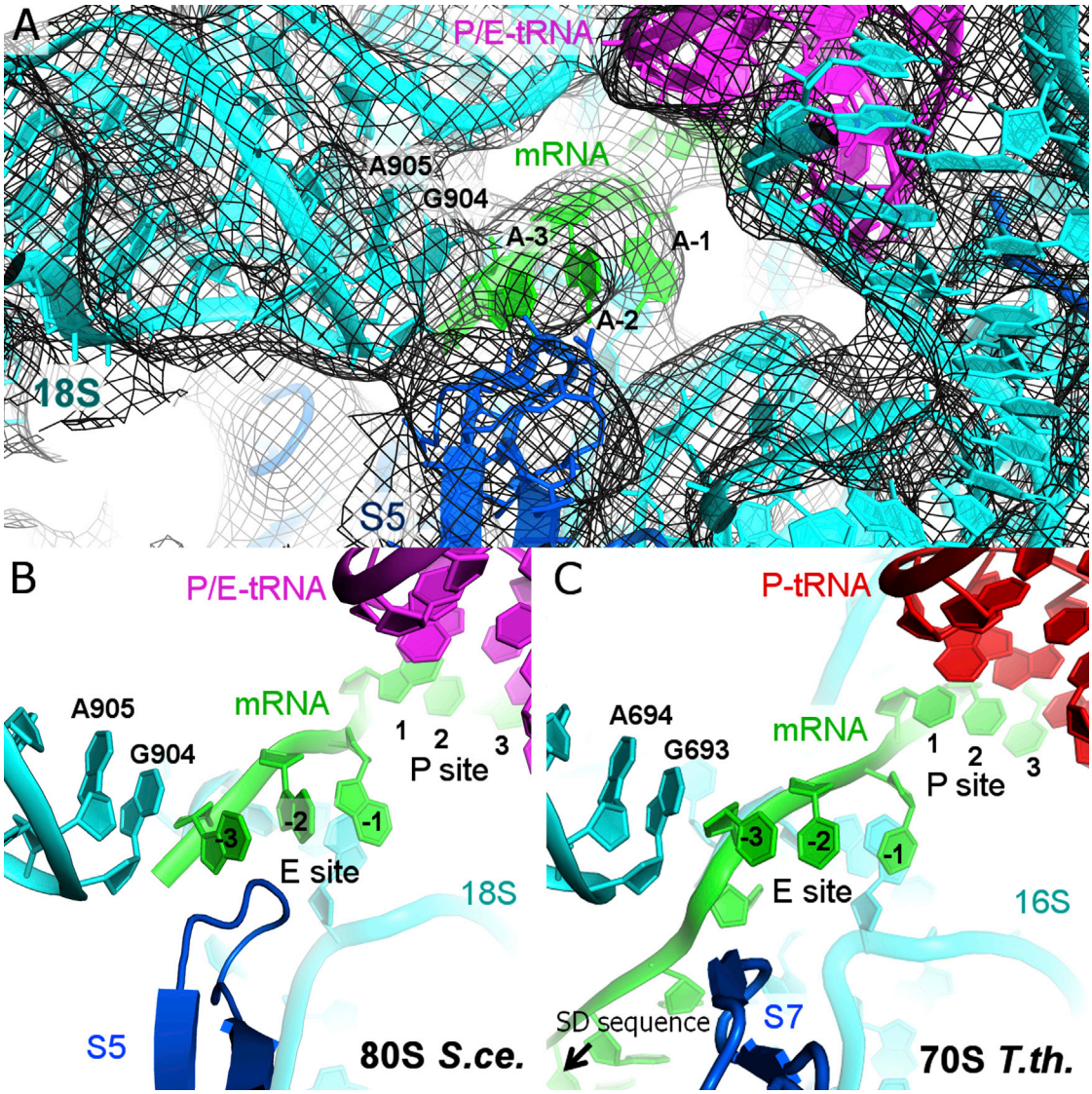

Figure 4. Interactions of mRNA with the E and P Sites of the 40S Subunit

(A) Fit of the molecular structure of the 80S bound with single tRNA into cryo-EM density.

(B) Interactions of mRNA with the elements of the 40S subunit and the anticodon stem loop of tRNA in the P site (this work). *S. ce*., *S. cerevisiae*.

(C) Interactions of mRNA in the 3.1 Å crystal structure of *T. thermophilus* (*T. th*.) 70S ribosome (PDB ID 3I8G; Jenner et al., 2010). Small-subunit rRNA is shown in cyan, mRNA in green, P/E-site tRNA in magenta, P-site tRNA in red, and ribosomal proteins in marine.

Visualization of the AAA trinucleotide preceding the AUG codon provides insights into the critical role that nucleotide A-3 plays in selecting an authentic start codon during initiation. Interactions of a purine residue with G904 and S5 during initiation likely stabilize the position of the mRNA in this region. Purine-purine stacking may provide up to 10-fold stronger binding than pyrimidine-purine stacking (Friedman and Honig, 1995), suggesting that a pyrimidine at −3 would result in less stable interactions with G904. Therefore, the conserved G904 of the 18S rRNA forms a stacking foundation to support the placement of A-3 or G-3 in the E site, resulting in proper positioning of downstream nucleotides. Interactions of S5 with A-3 may also contribute to stabilization of the Kozak sequence (Figure 4A). Together, the three nucleotides in the E site likely act as a molecular ruler to position the following AUG start codon in the P site, allowing the stable initiation complex to form.

EXPERIMENTAL PROCEDURES

Vacant 80S ribosomes were purified from *S. cerevisiae* strain W303 as described previously (Ben-Shem et al., 2011). 80S ribosome complexes were assembled in the presence of initiator *E. coli* $tRNA^{fMet}$ (ChemBlock), and an mRNA fragment (A**A**AAAUGUAAAAAA, Integrated DNA Technologies) containing the start codon AUG (underlined) and adenosine at position −3 (bold and underlined) characteristic for the *S. cerevisiae* Kozak fragment. Cryo-EM imaging was performed essentially as described previously (Koh et al., 2014). Image processing was performed essentially as described

previously (Brilot et al., 2013; Grigorieff, 2007). The initial data set consisted of 86,866 particles. Particles belonging to the two highest-resolution classes were refined using FREALIGN and optimal filtering (Sindelar and Grigorieff, 2011). 25,136 particles were extracted from the larger data set for further refinement to yield the reconstruction occupied with one tRNA. 23136 particles were extracted from the larger data set for further refinement to yield the reconstruction with two tRNAs. The 80S•tRNA and 80S•2tRNA structures were refined independently against the reconstructions (maps) employing stereochemically restrained real-space refinement essentially as described previously (Koh et al., 2014). Real-space R factors are 0.2 for both refined all-atom structures, indicating a good fit of the models to the maps. Details of ribosome sample formation; cryo-EM data collection; and processing, fitting, and refinement of structural models are described in the Supplemental Experimental Procedures.

ACCESSION NUMBERS

Cryo-EM maps and structural models have been deposited into the EMDataBank (IDs 5976 and 5977) and into the Research Collaboratory for Structural Bioinformatics (RCSB) (PDB IDs 3J77 and 3J78), respectively.

SUPPLEMENTAL INFORMATION

Supplemental Information includes Supplemental Experimental Procedures and two figures and can be found with this article online at http://dx.doi.org/10.1016/j.str.2014.06.003.

AUTHOR CONTRIBUTIONS

E.S., A.F.B., N.G., and A.A.K. designed the project. C.S.K. prepared purified ribosomes. E.S. prepared ribosome complexes. A.F.B. collected cryo-EM images. A.F.B and N.G. analyzed cryo-EM data. E.S. and A.A.K. built and refined structural models. All authors contributed to structure analysis and manuscript writing.

ACKNOWLEDGMENTS

We thank Allan Jacobson for providing a *S. cerevisiae* strain, Rohini Madireddy for help with protein purification, Zhiheng Yu and Jason de la Cruz for help with collecting data on the Titan Krios microscope, and Sarah Stumper for help with picking particles and initial steps of image processing. This study was supported by grants from the Worcester Foundation for Biomedical Research, by the UMMS Center for AIDS Research (to A.A.K), by NIH Grants R01 GM106105 (to A.A.K.) and P01 GM62580 (to N.G.), and by NSERC (to A.F.B.).

Received: April 22, 2014
Revised: May 28, 2014
Accepted: June 4, 2014
Published: July 17, 2014

REFERENCES

Agirrezabala, X., Lei, J., Brunelle, J.L., Ortiz-Meoz, R.F., Green, R., and Frank, J. (2008). Visualization of the hybrid state of tRNA binding promoted by spontaneous ratcheting of the ribosome. Mol. Cell *32*, 190–197.

Agirrezabala, X., Liao, H.Y., Schreiner, E., Fu, J., Ortiz-Meoz, R.F., Schulten, K., Green, R., and Frank, J. (2012). Structural characterization of mRNA-tRNA translocation intermediates. Proc. Natl. Acad. Sci. USA *109*, 6094–6099.

Aitken, C.E., and Lorsch, J.R. (2012). A mechanistic overview of translation initiation in eukaryotes. Nat. Struct. Mol. Biol. *19*, 568–576.

Anger, A.M., Armache, J.P., Berninghausen, O., Habeck, M., Subklewe, M., Wilson, D.N., and Beckmann, R. (2013). Structures of the human and Drosophila 80S ribosome. Nature *497*, 80–85.

Ben-Shem, A., Garreau de Loubresse, N., Melnikov, S., Jenner, L., Yusupova, G., and Yusupov, M. (2011). The structure of the eukaryotic ribosome at 3.0 Å resolution. Science *334*, 1524–1529.

Brilot, A.F., Korostelev, A.A., Ermolenko, D.N., and Grigorieff, N. (2013). Structure of the ribosome with elongation factor G trapped in the pretranslocation state. Proc. Natl. Acad. Sci. USA *110*, 20994–20999.

Budkevich, T., Giesebrecht, J., Altman, R.B., Munro, J.B., Mielke, T., Nierhaus, K.H., Blanchard, S.C., and Spahn, C.M. (2011). Structure and dynamics of the mammalian ribosomal pretranslocation complex. Mol. Cell *44*, 214–224.

Caulfield, T.R., Devkota, B., and Rollins, G.C. (2011). Examinations of tRNA Range of Motion Using Simulations of Cryo-EM Microscopy and X-Ray Data. J. Biophys. *2011*, 219515.

Cavener, D.R., and Ray, S.C. (1991). Eukaryotic start and stop translation sites. Nucleic Acids Res. *19*, 3185–3192.

Cornish, P.V., Ermolenko, D.N., Noller, H.F., and Ha, T. (2008). Spontaneous intersubunit rotation in single ribosomes. Mol. Cell *30*, 578–588.

Cornish, P.V., Ermolenko, D.N., Staple, D.W., Hoang, L., Hickerson, R.P., Noller, H.F., and Ha, T. (2009). Following movement of the L1 stalk between three functional states in single ribosomes. Proc. Natl. Acad. Sci. USA *106*, 2571–2576.

Dalgarno, L., and Shine, J. (1973). Conserved terminal sequence in 18SrRNA may represent terminator anticodons. Nat. New Biol. *245*, 261–262.

Demeshkina, N., Repkova, M., Ven'yaminova, A., Graifer, D., and Karpova, G. (2000). Nucleotides of 18S rRNA surrounding mRNA codons at the human ribosomal A, P, and E sites: a crosslinking study with mRNA analogs carrying an aryl azide group at either the uracil or the guanine residue. RNA *6*, 1727–1736.

Dever, T.E., and Green, R. (2012). The elongation, termination, and recycling phases of translation in eukaryotes. Cold Spring Harb. Perspect. Biol. *4*, a013706.

Dunkle, J.A., Wang, L., Feldman, M.B., Pulk, A., Chen, V.B., Kapral, G.J., Noeske, J., Richardson, J.S., Blanchard, S.C., and Cate, J.H. (2011). Structures of the bacterial ribosome in classical and hybrid states of tRNA binding. Science *332*, 981–984.

Ermolenko, D.N., Majumdar, Z.K., Hickerson, R.P., Spiegel, P.C., Clegg, R.M., and Noller, H.F. (2007). Observation of intersubunit movement of the ribosome in solution using FRET. J. Mol. Biol. *370*, 530–540.

Fei, J., Kosuri, P., MacDougall, D.D., and Gonzalez, R.L., Jr. (2008). Coupling of ribosomal L1 stalk and tRNA dynamics during translation elongation. Mol. Cell *30*, 348–359.

Frank, J., and Agrawal, R.K. (2000). A ratchet-like inter-subunit reorganization of the ribosome during translocation. Nature *406*, 318–322.

Friedman, R.A., and Honig, B. (1995). A free energy analysis of nucleic acid base stacking in aqueous solution. Biophys. J. *69*, 1528–1535.

Gao, Y.G., Selmer, M., Dunham, C.M., Weixlbaumer, A., Kelley, A.C., and Ramakrishnan, V. (2009). The structure of the ribosome with elongation factor G trapped in the posttranslocational state. Science *326*, 694–699.

Grigorieff, N. (2007). FREALIGN: high-resolution refinement of single particle structures. J. Struct. Biol. *157*, 117–125.

Guo, Z., and Noller, H.F. (2012). Rotation of the head of the 30S ribosomal subunit during mRNA translocation. Proc. Natl. Acad. Sci. USA *109*, 20391–20394.

Hamilton, R., Watanabe, C.K., and de Boer, H.A. (1987). Compilation and comparison of the sequence context around the AUG startcodons in Saccharomyces cerevisiae mRNAs. Nucleic Acids Res. *15*, 3581–3593.

Jenner, L.B., Demeshkina, N., Yusupova, G., and Yusupov, M. (2010). Structural aspects of messenger RNA reading frame maintenance by the ribosome. Nat. Struct. Mol. Biol. *17*, 555–560.

Julián, P., Konevega, A.L., Scheres, S.H., Lázaro, M., Gil, D., Wintermeyer, W., Rodnina, M.V., and Valle, M. (2008). Structure of ratcheted ribosomes with tRNAs in hybrid states. Proc. Natl. Acad. Sci. USA *105*, 16924–16927.

Kaminishi, T., Wilson, D.N., Takemoto, C., Harms, J.M., Kawazoe, M., Schluenzen, F., Hanawa-Suetsugu, K., Shirouzu, M., Fucini, P., and Yokoyama, S. (2007). A snapshot of the 30S ribosomal subunit capturing mRNA via the Shine-Dalgarno interaction. Structure *15*, 289–297.

Koh, C.S., Brilot, A.F., Grigorieff, N., and Korostelev, A.A. (2014). Taura syndrome virus IRES initiates translation by binding its tRNA-mRNA-like structural

element in the ribosomal decoding center. Proc. Natl. Acad. Sci. USA. Published online June 9, 2014. http://dx.doi.org/10.1073/pnas.1406335111.

Korostelev, A., and Noller, H.F. (2007). Analysis of structural dynamics in the ribosome by TLS crystallographic refinement. J. Mol. Biol. *373*, 1058–1070.

Korostelev, A., Trakhanov, S., Laurberg, M., and Noller, H.F. (2006). Crystal structure of a 70S ribosome-tRNA complex reveals functional interactions and rearrangements. Cell *126*, 1065–1077.

Korostelev, A., Trakhanov, S., Asahara, H., Laurberg, M., Lancaster, L., and Noller, H.F. (2007). Interactions and dynamics of the Shine Dalgarno helix in the 70S ribosome. Proc. Natl. Acad. Sci. USA *104*, 16840–16843.

Kozak, M. (1986). Point mutations define a sequence flanking the AUG initiator codon that modulates translation by eukaryotic ribosomes. Cell *44*, 283–292.

Lyumkis, D., Brilot, A.F., Theobald, D.L., and Grigorieff, N. (2013). Likelihood-based classification of cryo-EM images using FREALIGN. J. Struct. Biol. *183*, 377–388.

Moazed, D., and Noller, H.F. (1989). Intermediate states in the movement of transfer RNA in the ribosome. Nature *342*, 142–148.

Myasnikov, A.G., Simonetti, A., Marzi, S., and Klaholz, B.P. (2009). Structure-function insights into prokaryotic and eukaryotic translation initiation. Curr. Opin. Struct. Biol. *19*, 300–309.

Petrov, A.S., Bernier, C.R., Gulen, B., Waterbury, C.C., Hershkovits, E., Hsiao, C., Harvey, S.C., Hud, N.V., Fox, G.E., Wartell, R.M., and Williams, L.D. (2014). Secondary structures of rRNAs from all three domains of life. PLoS ONE *9*, e88222.

Pettersen, E.F., Goddard, T.D., Huang, C.C., Couch, G.S., Greenblatt, D.M., Meng, E.C., and Ferrin, T.E. (2004). UCSF Chimera—a visualization system for exploratory research and analysis. J. Comput. Chem. *25*, 1605–1612.

Pisarev, A.V., Kolupaeva, V.G., Pisareva, V.P., Merrick, W.C., Hellen, C.U., and Pestova, T.V. (2006). Specific functional interactions of nucleotides at key -3 and +4 positions flanking the initiation codon with components of the mammalian 48S translation initiation complex. Genes Dev. *20*, 624–636.

Pulk, A., and Cate, J.H. (2013). Control of ribosomal subunit rotation by elongation factor G. Science *340*, 1235970.

Ratje, A.H., Loerke, J., Mikolajka, A., Brünner, M., Hildebrand, P.W., Starosta, A.L., Dönhöfer, A., Connell, S.R., Fucini, P., Mielke, T., et al. (2010). Head swivel on the ribosome facilitates translocation by means of intra-subunit tRNA hybrid sites. Nature *468*, 713–716.

Schmeing, T.M., Moore, P.B., and Steitz, T.A. (2003). Structures of deacylated tRNA mimics bound to the E site of the large ribosomal subunit. RNA *9*, 1345–1352.

Schuwirth, B.S., Borovinskaya, M.A., Hau, C.W., Zhang, W., Vila-Sanjurjo, A., Holton, J.M., and Cate, J.H. (2005). Structures of the bacterial ribosome at 3.5 A resolution. Science *310*, 827–834.

Selmer, M., Dunham, C.M., Murphy, F.V., 4th, Weixlbaumer, A., Petry, S., Kelley, A.C., Weir, J.R., and Ramakrishnan, V. (2006). Structure of the 70S ribosome complexed with mRNA and tRNA. Science *313*, 1935–1942.

Sindelar, C.V., and Grigorieff, N. (2011). An adaptation of the Wiener filter suitable for analyzing images of isolated single particles. J. Struct. Biol. *176*, 60–74.

Sonenberg, N., and Hinnebusch, A.G. (2009). Regulation of translation initiation in eukaryotes: mechanisms and biological targets. Cell *136*, 731–745.

Spahn, C.M., Gomez-Lorenzo, M.G., Grassucci, R.A., Jørgensen, R., Andersen, G.R., Beckmann, R., Penczek, P.A., Ballesta, J.P., and Frank, J. (2004). Domain movements of elongation factor eEF2 and the eukaryotic 80S ribosome facilitate tRNA translocation. EMBO J. *23*, 1008–1019.

Spiegel, P.C., Ermolenko, D.N., and Noller, H.F. (2007). Elongation factor G stabilizes the hybrid-state conformation of the 70S ribosome. RNA *13*, 1473–1482.

Tourigny, D.S., Fernández, I.S., Kelley, A.C., and Ramakrishnan, V. (2013). Elongation factor G bound to the ribosome in an intermediate state of translocation. Science *340*, 1235490.

Verrier, S.B., and Jean-Jean, O. (2000). Complementarity between the mRNA 5′ untranslated region and 18S ribosomal RNA can inhibit translation. RNA *6*, 584–597.

Yusupov, M.M., Yusupova, G.Z., Baucom, A., Lieberman, K., Earnest, T.N., Cate, J.H., and Noller, H.F. (2001). Crystal structure of the ribosome at 5.5 A resolution. Science *292*, 883–896.

Yusupova, G., Jenner, L., Rees, B., Moras, D., and Yusupov, M. (2006). Structural basis for messenger RNA movement on the ribosome. Nature *444*, 391–394.

Zhou, J., Lancaster, L., Donohue, J.P., and Noller, H.F. (2013). Crystal structures of EF-G-ribosome complexes trapped in intermediate states of translocation. Science *340*, 1236086.

Structure, Volume *22*

Supplemental Information

Structures of Yeast 80S Ribosome-tRNA Complexes in the Rotated and Nonrotated Conformations

Egor Svidritskiy, Axel F. Brilot, Cha San Koh, Nikolaus Grigorieff, Andrei A. Korostelev

Supplemental Figures

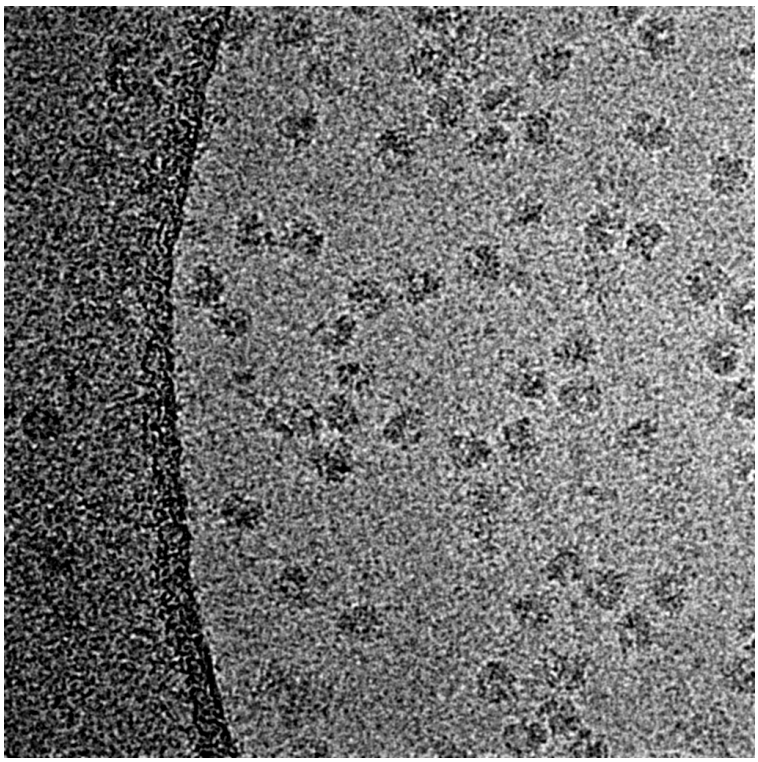

Figure S1, related to Figure 1. Cryo-EM micrograph showing 2D projections of yeast 80S ribosomes prepared with $tRNA^{fMet}$ and mRNA.

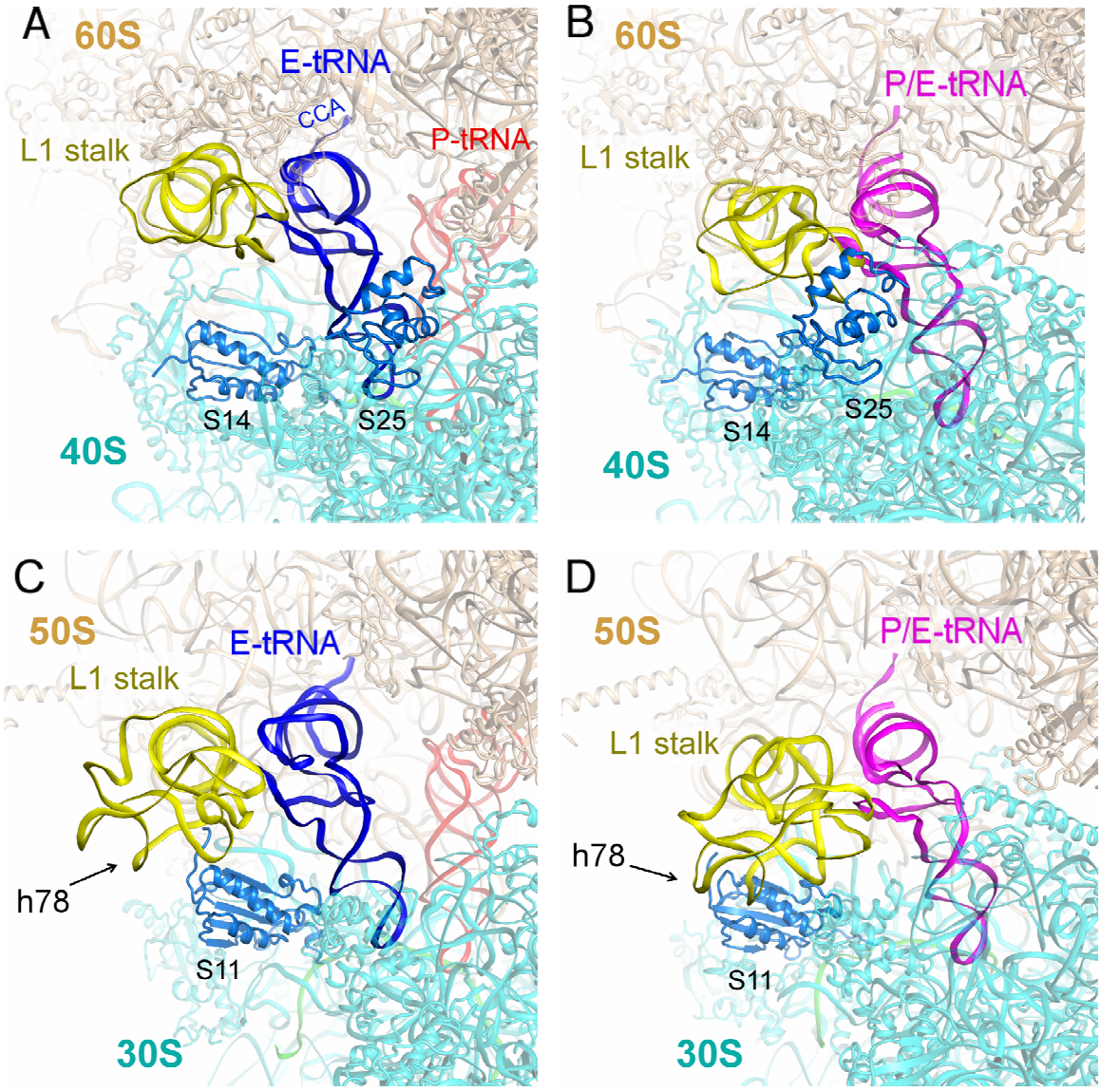

Figure S2, related to figures 2 and 3. Interactions of tRNA and L1 stalk in yeast and bacterial ribosomes. **A.** Interactions of E-tRNA and the L1 stalk in the non-rotated 80S•2tRNA structure (this work). In the non-rotated state, the L1 stalk does not contact the small ribosomal subunit. **B.** Interactions of P/E hybrid-state tRNA and the L1 stalk in the rotated 80S•tRNA structure (this work). Eukaryote-specific protein S25 approaches L1 stalk upon subunit rotation, so that the closest distance between protein backbone (Glu 45 region) and rRNA backbone (A2480 region) is reduced from ~40 Å (in the non-rotated state) to ~10 Å. **C.** Interactions of E-tRNA and the L1 stalk in the 70S•2tRNA structure PDB ID 3I9B and 3I9C) (Jenner et al., 2010). Unlike in the 80S•2tRNA structure, the L1 stalk is in the vicinity of the small subunit protein S11 due to the presence of helix 78, which is absent in the yeast ribosome. **D.** Interactions of P/E hybrid-state tRNA and the L1 stalk in the 70S•tRNA structure (PDB ID 3R8S and 4GD1) (Dunkle et al., 2011).

Supplemental Experimental Procedures

Ribosome complex formation

We assembled 80S ribosome complexes in the presence of initiator *E. coli* $tRNA^{fMet}$ (ChemBlock) and an mRNA fragment (A**A**AAAUGUAAAAAA, IDT) containing the start codon AUG (underlined) and adenosine at position -3 (bold and underlined) characteristic for the *S. cerevisiae* Kozak fragment. Bacterial $tRNA^{fMet}$ was previously shown to be fully functional in the puromycin and termination assays on the 80S ribosome (Frolova et al., 1996; Zhouravleva et al., 1995), consistent with the fact that tRNAs are functional in heterologous systems (Berthelot et al., 1973; Laycock and Hunt, 1969). The aim of the study was to visualize 80S termination complexes in the presence of release factors eRF1 and eRF3. Upon particle visualization, however, the high-resolution classes were found to not contain eRF1 or eRF3. Vacant 80S ribosomes were purified from *Saccharomyces cerevisiae* strain W303, following glucose starvation as described (Ben-Shem et al., 2011). Yeast eRF1 and eRF3 were purified as described (Shoemaker and Green, 2011). 0.3 uM 80S ribosome sample was mixed with 30 uM mRNA, 0.75 uM $tRNA^{fMet}$, 1 mM GppCp (Cell Signaling), 5 uM yeast eRF1 and 25 uM yeast eRF3 in buffer A (pH 7.5; 20 mM Tris-HCl, 50 mM NH_4Cl, 20 mM $MgCl_2$ and 0.3 U/ul RNasin (Promega)). All concentrations are specified for the final sample. The sample was incubated at 30^{o}C for one hour and then was flash-frozen.

Grids for electron cryomicroscopy were prepared essentially as described (Brilot et al., 2013), with minor modifications. Ribosomal complexes were thawed on ice immediately prior to plunging. Approximately 2 µL of undiluted sample was applied to freshly glow-discharged 400-mesh C-flat 1.2-1.3 grids using an FEI Mark II Vitrobot.

Electron Microscopy

Sample imaging was performed essentially as previously described (Brilot et al., 2013). Briefly, micrographs were collected on an FEI Titan Krios operating at 300 kV, and with a corrected spherical aberration of 0.01 mm. The nominal defocus was varied from 2.0 to 3.5 µm underfocus. Images were collected on a Falcon I direct electron detector, with a total dose of 30 electrons/Å^2, and a calibrated pixel size on the specimen of 1.05 Å. A total of 4754 micrographs were collected.

Image Processing

Image processing was performed essentially as described (Brilot et al., 2013; Grigorieff, 2007). Particles were semi-automatically selected using e2boxer's swarm tool (Tang et al., 2007), followed by manual curation of the dataset. Defocus parameters were determined using CTFFIND3 (Mindell and Grigorieff, 2003). Boxing was performed using batchboxer (Ludtke et al., 1999) , with unbinned images having a box size of 360 pixels. The initial dataset consisted of 86866 particles.

Initial alignment parameters were assigned using IMAGIC (Van Heel et al., 2011), essentially as described (Brilot et al., 2013). Boxed particles were normalized to

have a constant variance and zero average, 5-fold binned, phase flipped to account for the contrast transfer function (CTF), band-pass filtered with cut-offs of 0.03 and 0.33, and masked with a soft circular mask with radius 0.62 (fraction of half the image size) and a fall-off of 0.08. Particle images were aligned against reprojections of a published 80S ribosome structure (Schuler et al., 2006) (EMD-1285). Further processing with FREALIGN (Grigorieff, 2007) was carried out essentially as described (Brilot et al., 2013) using unfiltered images. The data was refined against a single reference until no further improvement was seen in resolution as indicated by the calculated Fourier shell correlation (FSC) between rounds. Refinement included data up to 35 Å initially, and data at higher resolution as refinement progressed, up to a resolution of 10 Å in the final round of refinement. Classification into five classes was performed on two-fold binned data, where the initial class occupancies were randomly assigned using RSAMPLE (Lyumkis et al., 2013). Classification was performed without refining the alignment parameters, including data between 150 and 14 Å for 52 cycles, followed by five cycles where the alignment parameters and occupancies were jointly refined. This yielded two high quality classes with recognizable features at high resolution (Rosenthal and Henderson, 2003) (better than 10 Å, FSC = 0.143).

Particles belonging to the two highest resolution classes (occupancy > 70%) were then extracted from the dataset, and further refined against a single reference using FREALIGN and optimal filtering (Sindelar and Grigorieff, 2012). 25136 particles were extracted from the larger dataset for further refinement to yield the reconstruction occupied with one tRNA. 23136 particles were extracted from the larger dataset for further refinement to yield the reconstruction with two tRNAs. The refinement included data from 150 to 14 Å initially, and up to a resolution of 10 Å in the final rounds of refinement. Data beyond 10 Å resolution was never used during refinement and classification to ensure resolution estimation that is not affected by noise overfitting.

The resolution of the classes (Fig. 1E) was assessed using half-volumes generated by FREALIGN and subsequent masking. Briefly, a generous mask with a 7-pixel fall-off was generated from the final volumes using the automask3d command implemented in EMAN2 (Tang et al., 2007), and applied to both half volumes prior to determination of the FSC (curved labeled “with masking” in Fig. 1E). Additionally, FSC curves generated by FREALIGN are shown (Fig. 1E) that take into account the noise added by the solvent surrounding the particle to give a more accurate resolution estimate of the density within the particle (Sindelar and Grigorieff, 2012).

Fitting of tRNA-bound 80S structural models into cryo-EM maps

The 3.0-Å crystal structure of the 80S ribosome (Ben-Shem et al., 2011) was fitted into the cryo-EM maps using Chimera and then $tRNA^{fMet}$ and mRNA were modeled using individual tRNA and mRNA from the crystal structures of the hybrid-state 70S ribosome containing P/E tRNA (Dunkle et al., 2011) or non-rotated 70S ribosome containing tRNAs in the P and E sites (Jenner et al., 2010; Korostelev et al., 2008). The 80S•tRNA and 80S•2tRNA structures were

independently refined against the maps, using the stereochemically-restrained rigid-body real-space refinement package RSRef (Chen et al., 2003; Fabiola and Chapman, 2005; Korostelev et al., 2002), implemented as a module of CNS (Brunger et al., 1998), essentially as described (Koh et al., 2014). The structure of rpL1 was obtained by homology modeling from PDB ID 3J3B (Anger et al., 2013), using the SWISS-MODEL server (Arnold et al., 2006). At the last stage of structure optimization, the structural models were subject to stereochemically-restrained all-atom real-space refinement against cryo-EM maps, facilitated by secondary-structure restraints (base-pairing, base-stacking and intra-protein hydrogen-bonding) as described (Laurberg et al., 2008). Real-space R-factors, calculated in RSRef and reporting on disagreement between the structural model and experimental maps, are 0.2 for both refined all-atom structures, indicating good fit of the models to the map. All-atom root-mean-square differences between 25S rRNA of the refined structures and the starting 3-Å crystal structure (PDB ID 3U5D, excluding the mobile L1 stalk, P stalk and the A-site finger) are 1.1 Å for both 80S complexes. This is consistent with the average coordinate error of ~1 Å for the refined structural models, similar to the expected coordinate error of a cryo-EM structure at ~6 Å resolution (Rossmann, 2000). Structural alignments were performed in Pymol (DeLano, 2002). Figures were rendered in Pymol and Chimera (Pettersen et al., 2004).

REFERENCES

Anger, A. M., Armache, J. P., Berninghausen, O., Habeck, M., Subklewe, M., Wilson, D. N., and Beckmann, R. (2013). Structures of the human and Drosophila 80S ribosome. Nature *497*, 80-85.

Arnold, K., Bordoli, L., Kopp, J., and Schwede, T. (2006). The SWISS-MODEL workspace: a web-based environment for protein structure homology modelling. Bioinformatics *22*, 195-201.

Ben-Shem, A., Garreau de Loubresse, N., Melnikov, S., Jenner, L., Yusupova, G., and Yusupov, M. (2011). The structure of the eukaryotic ribosome at 3.0 A resolution. Science *334*, 1524-1529.

Berthelot, F., Bogdanovsky, D., Schapira, G., and Gros, F. (1973). Interchangeability of factors and tRNA's in bacterial and eukaryotic translation initiation systems. Mol Cell Biochem *1*, 63-72.

Brilot, A. F., Korostelev, A. A., Ermolenko, D. N., and Grigorieff, N. (2013). Structure of the ribosome with elongation factor G trapped in the pretranslocation state. Proc Natl Acad Sci U S A.

Brunger, A. T., Adams, P. D., Clore, G. M., DeLano, W. L., Gros, P., Grosse-Kunstleve, R. W., Jiang, J. S., Kuszewski, J., Nilges, M., Pannu, N. S.*, et al.* (1998). Crystallography & NMR system: A new software suite for macromolecular structure determination. Acta Crystallogr D Biol Crystallogr *54*, 905-921.

Chen, J. Z., Furst, J., Chapman, M. S., and Grigorieff, N. (2003). Low-resolution structure refinement in electron microscopy. J Struct Biol *144*, 144-151.

DeLano, W. L. (2002). The PyMOL Molecular Graphics System (Palo Alto, CA, USA.: DeLano Scientific).

Dunkle, J. A., Wang, L., Feldman, M. B., Pulk, A., Chen, V. B., Kapral, G. J., Noeske, J., Richardson, J. S., Blanchard, S. C., and Cate, J. H. (2011). Structures of the bacterial ribosome in classical and hybrid states of tRNA binding. Science *332*, 981-984.

Fabiola, F., and Chapman, M. S. (2005). Fitting of high-resolution structures into electron microscopy reconstruction images. Structure *13*, 389-400.

Frolova, L., Le Goff, X., Zhouravleva, G., Davydova, E., Philippe, M., and Kisselev, L. (1996). Eukaryotic polypeptide chain release factor eRF3 is an eRF1- and ribosome-dependent guanosine triphosphatase. RNA *2*, 334-341.

Grigorieff, N. (2007). FREALIGN: High-resolution refinement of single particle structures. Journal of Structural Biology *157*, 117-125.

Jenner, L. B., Demeshkina, N., Yusupova, G., and Yusupov, M. (2010). Structural aspects of messenger RNA reading frame maintenance by the ribosome. Nat Struct Mol Biol *17*, 555-560.

Koh, C. S., Brilot, A. F., Grigorieff, N., and Korostelev, A. A. (2014). Taura syndrome virus IRES initiates translation by binding its tRNA-mRNA–like structural element in the ribosomal decoding center. Proc Natl Acad Sci U S A.

Korostelev, A., Asahara, H., Lancaster, L., Laurberg, M., Hirschi, A., Zhu, J., Trakhanov, S., Scott, W. G., and Noller, H. F. (2008). Crystal structure of a translation termination complex formed with release factor RF2. Proc Natl Acad Sci U S A *105*, 19684-19689.

Korostelev, A., Bertram, R., and Chapman, M. S. (2002). Simulated-annealing real-space refinement as a tool in model building. Acta Crystallogr D Biol Crystallogr *58*, 761-767.

Laurberg, M., Asahara, H., Korostelev, A., Zhu, J., Trakhanov, S., and Noller, H. F. (2008). Structural basis for translation termination on the 70S ribosome. Nature *454*, 852-857.

Laycock, D. G., and Hunt, J. A. (1969). Synthesis of rabbit globin by a bacterial cell free system. Nature *221*, 1118-1122.

Ludtke, S. J., Baldwin, P. R., and Chiu, W. (1999). EMAN: Semiautomated Software for High-Resolution Single-Particle Reconstructions. Journal of Structural Biology *128*, 82-97.

Lyumkis, D., Brilot, A. F., Theobald, D. L., and Grigorieff, N. (2013). Likelihood-based classification of cryo-EM images using FREALIGN. J Struct Biol *183*, 377-388.

Mindell, J. A., and Grigorieff, N. (2003). Accurate determination of local defocus and specimen tilt in electron microscopy. Journal of Structural Biology *142*, 334-347.

Pettersen, E. F., Goddard, T. D., Huang, C. C., Couch, G. S., Greenblatt, D. M., Meng, E. C., and Ferrin, T. E. (2004). UCSF Chimera--a visualization system for exploratory research and analysis. J Comput Chem *25*, 1605-1612.

Rosenthal, P. B., and Henderson, R. (2003). Optimal determination of particle orientation, absolute hand, and contrast loss in single-particle electron cryomicroscopy. Journal of molecular biology *333*, 721-745.

Rossmann, M. G. (2000). Fitting atomic models into electron-microscopy maps. Acta Crystallogr D Biol Crystallogr *56*, 1341-1349.

Schuler, M., Connell, S. R., Lescoute, A., Giesebrecht, J., Dabrowski, M., Schroeer, B., Mielke, T., Penczek, P. A., Westhof, E., and Spahn, C. M. (2006). Structure of the ribosome-bound cricket paralysis virus IRES RNA. Nat Struct Mol Biol *13*, 1092-1096.

Shoemaker, C. J., and Green, R. (2011). Kinetic analysis reveals the ordered coupling of translation termination and ribosome recycling in yeast. Proc Natl Acad Sci U S A *108*, E1392-1398.

Sindelar, C. V., and Grigorieff, N. (2012). An adaptation of the Wiener filter suitable for analyzing images of isolated single particles. J Struct Biol *176*, 60-74.

Tang, G., Peng, L., Baldwin, P. R., Mann, D. S., Jiang, W., Rees, I., and Ludtke, S. J. (2007). EMAN2: An extensible image processing suite for electron microscopy. Journal of Structural Biology *157*, 38-46.

Van Heel, M., Portugal, R., Rohou, A., Linnemayr, C., Bebeacua, C., Schmidt, R., Grant, T., and Schatz, M. (2011). Four-dimensional cryo electron microscopy at quasi atomic resolution:'IMAGIC 4D'. International tables for crystallography Vol F: Crystallography of biological macromolecules, 624-628.

Zhouravleva, G., Frolova, L., Le Goff, X., Le Guellec, R., Inge-Vechtomov, S., Kisselev, L., and Philippe, M. (1995). Termination of translation in eukaryotes is governed by two interacting polypeptide chain release factors, eRF1 and eRF3. Embo J *14*, 4065-4072.